2nd Advanced Optical Metrology Compendium

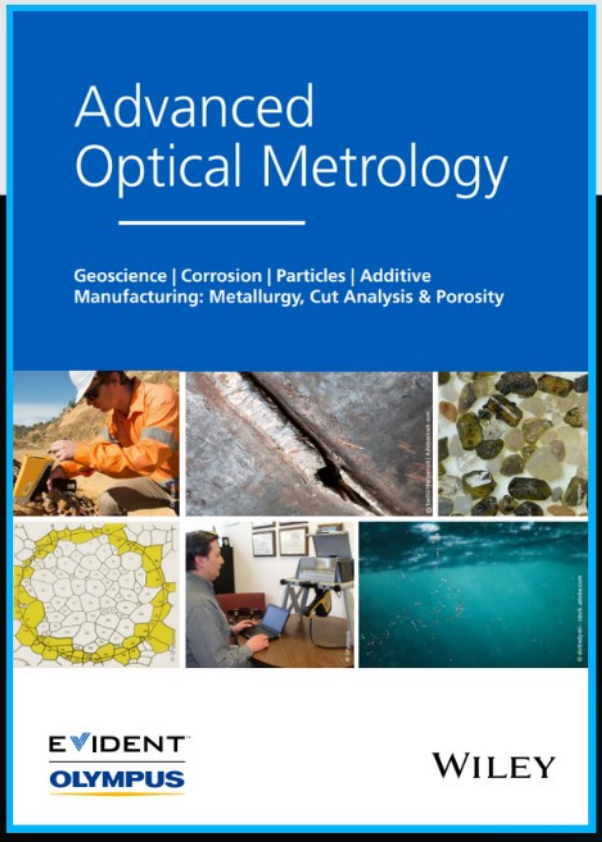

The latest eBook from Advanced Optical Metrology. Download for free.

This compendium includes a collection of optical metrology papers, a repository of teaching materials, and instructions on how to publish scientific achievements.

With the aim of improving communication between fundamental research and industrial applications in the field of optical metrology we have collected and organized existing information and made it more accessible and useful for researchers and practitioners.

EVIDENT
OLYMPUS

WILEY

NANO · MICRO small
www.small-journal.com

Nanocarriers Made of Proteins: Intracellular Visualization of a Smart Biodegradable Drug Delivery System

*Marie-Luise Frey, Shen Han, Henry Halim, Anke Kaltbeitzel, Andreas Riedinger, Katharina Landfester, and Ingo Lieberwirth**

This work analyzes the intracellular fate of protein-based nanocarriers along their endolysosomal pathway by means of correlative light and electron microscopy methods. To unambiguously identify the nanocarriers and their degradation remnants in the cellular environment, they are labeled with fluorescent, inorganic nanoplatelets. This allows tracking the nanocarriers on their intracellular pathway by means of electron microscopy imaging. From the present data, it is possible to identify different cell compartments in which the nanocarriers are processed. Finally, three different terminal routes for the intracellular destiny of the nanocarriers are presented. These findings are important to reveal the degradation process of protein nanocapsules and contribute to the understanding of the therapeutic success of an encapsulated drug.

1. Introduction

The use of nanocarriers for drug delivery is becoming increasingly popular in medical research.[1,2] Besides liposomes and nanoparticles, which already find applications in clinics, core–shell structures like NCs are also appropriate candidates for the use as drug delivery platform.[3–6] Especially NCs made from proteins have many advantages, such as their biodegradability, high loading capacity with a combination of hydrophilic drugs and low toxicity.[7,8] Due to their size, nanocarriers (NCs) can permeate cells easily and therefore it is of great importance to elucidate how the uptake and the further fate of the nanocarrier in the cell occur.[9]

Nanocarriers are usually processed along the endolysosomal pathway.[10] However, polymeric NCs, such as protein NCs, are hard to track within this pathway since they cannot be clearly identified: they require either fluorescent markers to be observed by light microscopy (LM) or electron-dense markers to be observed by electron microscopy (EM). Correlative light and electron microscopy (CLEM) combine the strengths of both techniques and contribute to a precise localization of the nanocarriers in the cell. Using fluorescent nanodiamonds, for example, can serve as a fluorescent marker[11,12] These markers have the advantage of being biocompatible and can be easily modified to achieve a certain surface functionalization.[13] CLEM preparation ideally features a fluorophore with a stable inherent fluorescence suitable for confocal laser scanning microscopy (cLSM) which, in combination, has a contrasting component suitable for transmission electron microscopy (TEM). Another approach is using inorganic, fluorescent nanoparticles. Quantum dots are the commonly used fluorescent markers for intracellular tracking, but they are not as bright as NPLs for both one photon and two photon excitation.[19] Moreover, due to their small size and spherical shape it can be challenging to identify quantum dots—but also the larger, rectangular NPLs—in a cellular environment by TEM.[14,15] This might involve additional elemental analysis (e.g., energy dispersive x-ray spectroscopy [EDS] or electron energy loss spectroscopy [EELS]) to confirm the identity of the quantum dots to ultimately locate the nanocarrier.[16–18]

Here, we develop a model system consisting of an organic nanocapsule (NC) labeled with a fluorescent labeling system. As fluorescent marker we utilize large (20–50 nm), rectangular CdSe-CdZnS nanoplatelets (NPLs). We encapsulated these NPLs into biocompatible NCs by a polyaddition reaction at the droplet interface in an inverse miniemulsion. We used NCs made of bovine serum albumin (BSA), crosslinked at the interface with toluene diisocyanate (TDI), forming a dense polymeric shell.[6,7] The NPLs were added to the aqueous dispersed phase during the miniemulsion process, leading to the encapsulation of the NPLs into the NCs. The key to success of the NPL markers hinged on the protective coating on the NPLs.[19] This coating makes NPLs both easy to disperse in aqueous medium and protects the NPLs' surface from major damage during the encapsulation process, thus leading to high fluorescence after encapsulation. The potential toxicity of CdSe nanoparticles is not an issue at this stage. The fluorescent marker can either be easily replaced or even omitted completely.

To follow the intracellular pathway of the protein NCs, RAW264.7 macrophages were incubated with these NCs followed by different techniques like flow cytometry, cLSM, and

M.-L. Frey, S. Han, H. Halim, A. Kaltbeitzel, A. Riedinger, K. Landfester, I. Lieberwirth
Max Planck Institute for Polymer Research
Ackermannweg 10, 55128 Mainz, Germany
E-mail: lieberw@mpip-mainz.mpg.de

The ORCID identification number(s) for the author(s) of this article can be found under https://doi.org/10.1002/smll.202106094.

DOI: 10.1002/smll.202106094

electron microscopy. After incubation, the NCs were intracellularly localized revealing different terminal destinations along the endolysosomal pathway involving early and late endosomes and endolysosomes. This information about the intracellular behavior of BSA nanocapsules is extremely important for the development of new protein-based nanocarriers as drug delivery systems.

2. Results and Discussion

We used the miniemulsion method to synthesize protein NCs made of BSA,[7] loaded with NPLs. We accomplished the loading of the NPLs into biocompatible NCs by adding water-dispersible NPLs to the aqueous phase of a miniemulsion. The number of NPLs per nanodroplet of the miniemulsion—the precursor for the subsequent NCs—is assumed to follow a Poisson distribution. Hence, we employed an excess of NPLs per expected NC to achieve a labeling of all capsules (exemplary calculation in Supporting Information, Table S1 and Equation S1 in Supporting Information) with at least one NPL. In addition, we synthesized a 1:1 ratio (NPLs:NCs) and NCs without NPLs to uncover any changes of the capsule properties due to excess NPLs.

After the NPLs have been evenly dispersed in the aqueous phase, BSA was added followed by emulsification in cyclohexane in the presence of the surfactant poly-((ethylene-*co*-butylene)-*b*-(ethylene oxide) (P(E/B)-*b*-EO)).[20] The final step to obtain the BSA NCs is the addition of a crosslinker TDI, which reacts in a polyaddition reaction at the droplet interface and leads to a shell made of crosslinked BSA on the water–cyclohexane interphase.

However, in order to use these NCs for biomedical applications, they need to be transferred to an aqueous phase (**Figure 1**A) by replacing the cyclohexane with water. This is achieved by redispersing the NCs in aqueous sodiumdodecylsulfate (SDS) solution followed by evaporation of the cyclohexane.

We then analyzed the size distribution and hydrodynamic radii. Three different NPL:NC ratios and one NC sample without NPLs were synthesized and the size distribution was measured in cyclohexane as well as in aqueous phase after the transfer of the NCs from the organic to the water phase. Furthermore, we analyzed the morphologies of the obtained BSA NCs in cyclohexane (Figure 1C) and in water (Figure 1D) by cryo-TEM. To check the suitability for cLEM measurements, we studied the photoluminescence of the BSA NCs with different NPLs loadings in cyclohexane (Figure 1E) and after redispersion to water (Figure 1F). The different relative fluorescence intensities can probably be attributed to two different effects. First, we have seen that free NPLs are present in cyclohexane, which are removed upon transfer to water (Figure 1C,E and Figure S3, Supporting Information). Second, we must assume that the transfer of cyclohexane into water is accompanied by a loss of NCs. Unfortunately, it is not yet entirely clear to what extent these two effects contribute to the observed shift in fluorescence intensities.

The average hydrodynamic radius (R_h) of the capsules with the different NPL loadings in cyclohexane is 153 ± 9 nm (Figure 1B), where the NCs without NPLs have the smallest R_h (141 ± 83 nm), while NCs with the 1:10 ratio of NPLs revealed the largest capsule R_h (163 ± 88 nm). These results point out, that BSA NC formation is not significantly influenced by the presence of NPLs. After transfer to the water phase we observed a moderate increase of the capsule radii ranging from 172 nm (without NPLs) to 218 nm (at a NC:NPL ratio of 1:1). The light scattering results clearly show the similarity of the NCs at the different NPL loadings with regards to size distribution. Zeta potentials were negative for all NCs (Figure 1B).

Cryo-TEM images confirm the colloid nature of the BSA NCs in both phases (Figure 1C,D and Figure S3, Supporting Information). In cyclohexane, the NCs appear like being deflated. This observation may be due to the different expansion coefficients of water and cyclohexane under cryo conditions. In the water phase, this effect is not that pronounced and the BSA NC has a more spherical shape. After the transfer to the water phase, each BSA NC contains at least one NPL (Figure S3D, Supporting Information). The cryo-TEM micrographs further illustrate how the visibility of NPLs depends on their orientation. Edge-on oriented NPLs show a very dark contrast and a typical rod-like shape. However, if the NPLs are in a flat-on orientation, they have a much weaker contrast in the TEM and are therefore hard to see, especially if they are in an NC or in a cellular environment. Leakage of NPLs from the BSA NCs is not observed.

We analyzed the fluorescence intensity of the BSA NCs in cyclohexane (Figure 1E) and in water (Figure 1F), revealing the fluorescence emission maximum at 646 nm in both cases. A reliable measurement of the absorption spectra of the encapsulated NPLs was not possible because the sample dispersion was too turbid. However, a thorough photophysical characterization of the NPLs can be found elsewhere.[19] As expected, the measured fluorescence intensity increases with increasing NPL concentration. After transfer to water, the capsules were again subjected to fluorescence intensity measurements, demonstrating similar fluorescence intensities for the 10:1 and the 5:1 ratio and a low fluorescence intensity for the 1:1 ratio. These observations corroborate that excess NPLs, which were not encapsulated, were removed during the water transfer process. This observation is corroborated by the cryo-TEM images in cyclohexane and in water (Figure S3, Supporting Information). In addition, we confirmed successful loading of the NPLs to the NCs by fluorescence quenching of fluorescein isothiocyanate (FITC) attached to the capsule surface.[21] The fluorescence quenching of the FITC increases with the number of encapsulated NPLs. This fluorescence quenching could suggest Förster resonance energy transfer (FRET) to nearby NPLs. Here, the NPLs act as acceptor and the FITC as donor. Previous studies of FRET with NPLs[22,23] determined Förster radii of just a few nm, indicating close proximity of the NPLs to the FITC attached to the thin capsule shell (Figure S1, Supporting Information). This indicates that the NPLs stay close to the capsule walls, rather than freely disperse outside or inside the capsule, where fluorescence quenching via FRET from the FITC to the NPLs would be less likely. Another quenching mechanism, although much weaker, could also be absorption of FITC emission by the NPLs since their spectral overlap is high. In addition, we did not observe NPLs in the supernatant of aqueous capsule dispersions, but the NPLs were always associated within the BSA

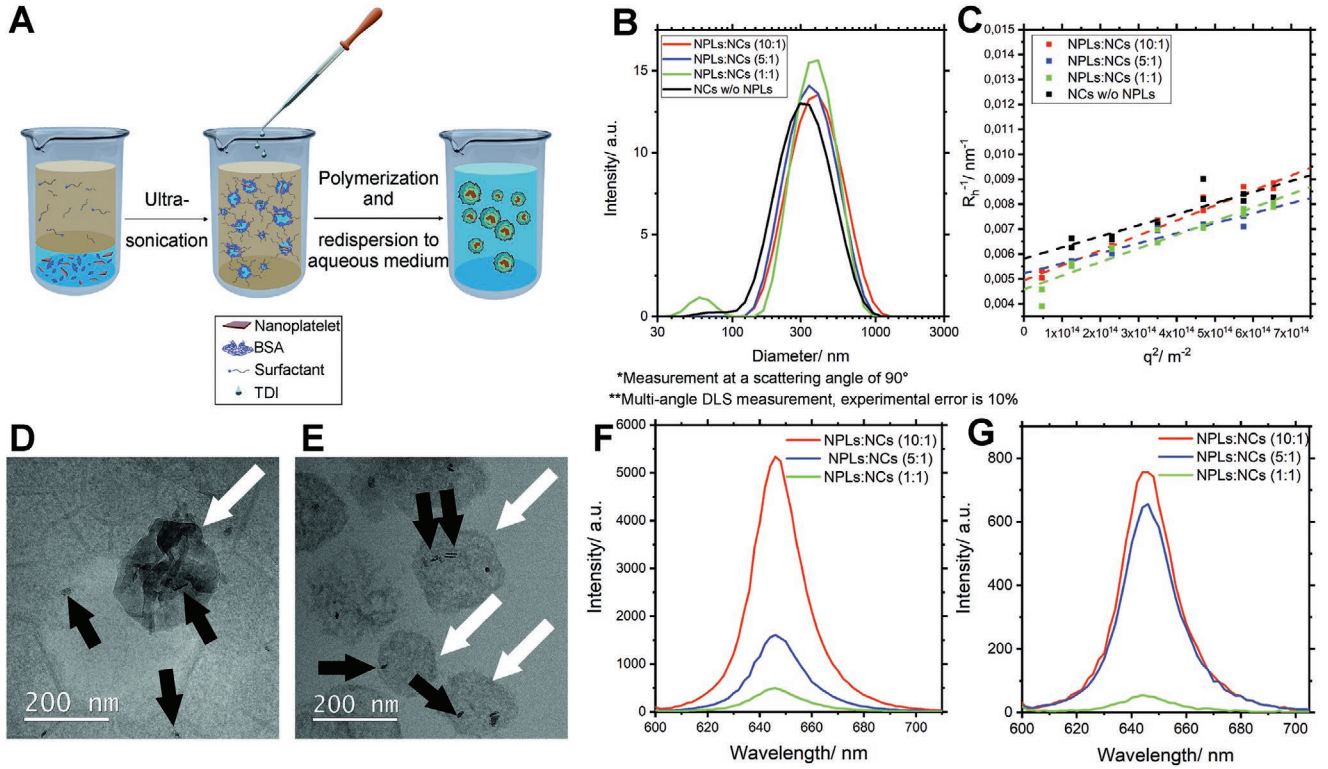

Figure 1. Characterization of BSA nanocapsules (NCs) loaded with different amounts of water-dispersible nanoplatelets (NPLs). A) Synthesis scheme for the inverse miniemulsion: BSA and the NPLs were dispersed in the aqueous (blue) phase, the surfactant is dissolved in the cyclohexane phase (light brown). After ultrasonication the miniemulsion is formed and the BSA is crosslinked at the droplet surface by adding TDI. Finally, the NCs are redispersed to an aqueous phase. B) DLS distribution curves of NCs encapsulating different NPL ratios in cyclohexane. C) Multi-angle light scattering measurements of the same NCs. Cryo-TEM image of a BSA NCs loaded with NPLs (5:1 ratio) D) in cyclohexane and E) in water. BSA NCs are indicated by white arrows, the NPLs by black arrows. F) Fluorescence intensity measurements of BSA NCs encapsulating different NPLs ratios in cyclohexane and G) after redispersion in water.

NCs. Based on these findings, we continued the cell experiments using freshly prepared BSA NCs adjusted at a 5:1 ratio.

In order to study the uptake behavior of the BSA NCs, RAW264.7 macrophages were exposed to BSA NCs for 1 h (**Figure 2**). The reason for the selection of macrophages is their ability to take up almost any external material. We analyzed time-dependent cell uptake by cLSM. Cells were treated with BSA NCs (75 µg mL^{-1}, + FBS) and identified by means of their fluorescence emission. We visualized lysosomal cell compartments using LysoTracker Green (Figure 2A) and correlated the measured fluorescence intensities to the BSA NCs signal (Figure 2B,C). The LysoTracker Green DND-26 marker stains acidic compartments, thus marking endolysosomal membranes.

We observed a low amount of intracellular NPLs after 4 min of incubation time, with almost a linear increase in uptake (Figure S2, Supporting Information) during the next 62 min for high (300 µg mL^{-1}) and low (75 µg mL^{-1}) loadings (Figure 2A,B). The NCs were transported during that time from the membrane into the cell where they gradually co-localize with endosomes/lysosomes marked by LysoTracker Green.

Throughout the uptake process, microscopic observation did not reveal any signs that might indicate cytotoxicity of the NCs. The NPLs are used for experimental purposes only and can simply be omitted in the application of the NCs. Hence, these do not need to be subjected to a detailed examination with regard to their cytotoxicity. But the use of the TDI as a crosslinker could have a negative impact on the viability of cells. However, in a very similar system using TDI crosslinked ovalbumin capsules, no increased cytotoxicity was observed.[24] Therefore, we can assume that the NCs used here are not cytotoxic and that all the TDI reacted off.

At the beginning of the incubation, there is almost no co-localization of the NPLs with LysoTracker since they were not yet transferred to the acidic compartments like late endosomes/lysosomes. Within the first 30 min, the fraction of NPLs that are found in late endosomes/lysosomes linearly increases. Despite linear uptake of NPLs with time over 60 min, we stopped live cell imaging to avoid phototoxicity having an impact on the uptake process. The M2 co-localization coefficient levels off after about 50 min (Figure 2C). Considering a continuous uptake of NCs, this leveling off can be interpreted as a reduction of endosome maturation to lysosomes or may indicate endosomal escape as NCs were continuously taken up (Figure 2B). Moreover, TEM images are used to corroborate this hypothesis.

To analyze NCs trafficking inside the cell, we incubated RAW264.7 macrophages with BSA NCs loaded with water-dispersible NPLs (5:1) at a concentration of 300 µg mL^{-1}. We exposed the macrophages to the NCs for 2 h, to ensure

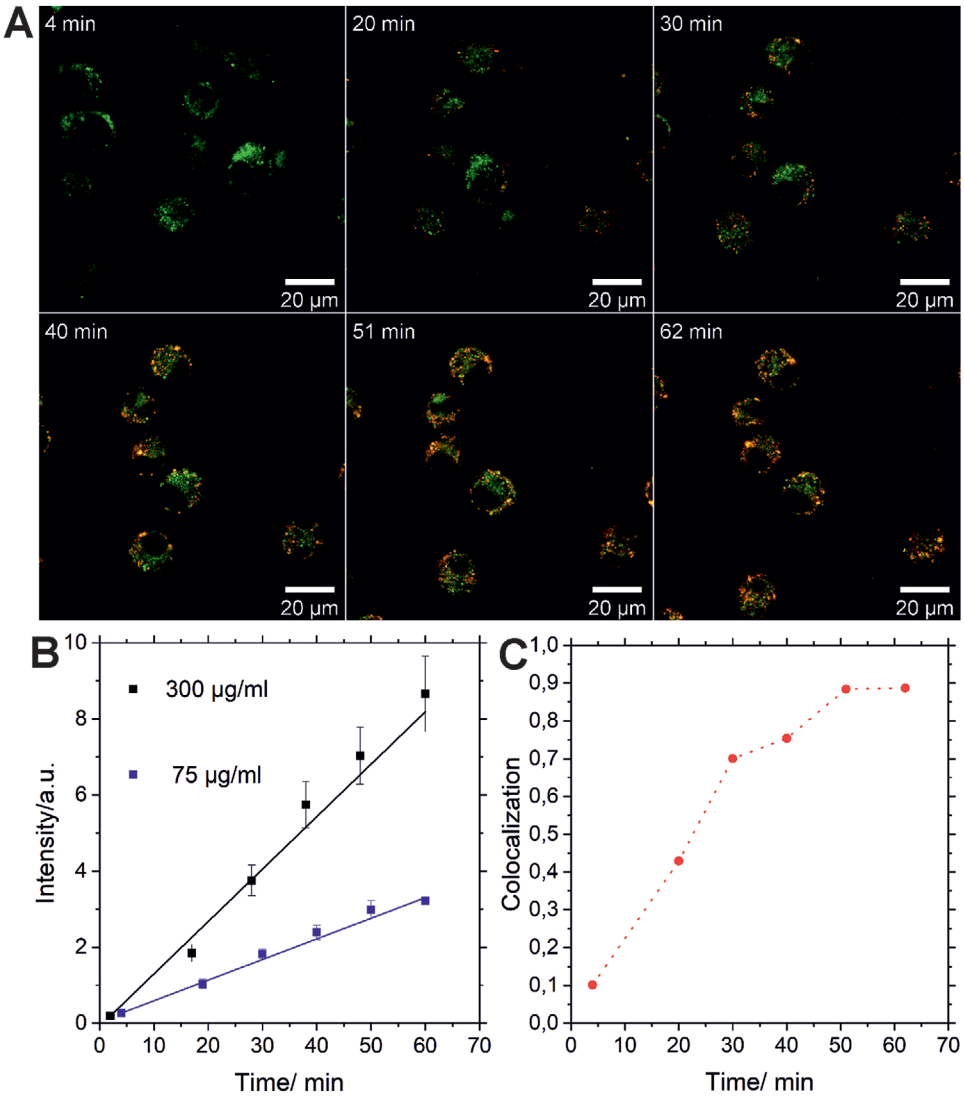

Figure 2. Cell uptake experiments of NPL loaded NCs (5:1) into RAW264.7 macrophages. A) Live cell imaging by confocal laser scanning microscopy (cLSM) of macrophages stained with LysoTracker Green after the uptake of NCs (NPL displayed in red) at a concentration of 75 µg mL^{-1}. B) Time-dependent increase of detected fluorescence intensity of NPLs encapsulated in BSA NCs in RAW264.7 macrophages. C) Time-dependent correlation of overlapping fluorescence signals obtained from the cLSM data (A) of the cell uptake of BSA NCs into macrophages determined by Manders (M2) coefficient. The M2 coefficient shows the fraction of NPLs that co-localize with endosomes/lysosomes. It ranges between 0 and 1.

sufficient and continuous uptake, and washed them to stop the uptake. Subsequently, they were allowed to ripe for another 24 h to allow processing of the NCs inside the cells (ripening time).

We performed CLEM on 100 nm sections to precisely localize intracellular BSA NCs in high resolution after being taken up. Initially, an ultrathin section of the cells was imaged by cLSM (Leica SP5, Germany) to obtain the fluorescence image of the region of interest (ROI). Then, the same sections were observed using a transmission electron microscope. Finally, the images from cLSM and TEM of the same ROI were then registered and overlaid to yield the correlative micrograph. It turns out that the fluorescence of the NPLs was preserved and could clearly be detected in cLSM even after the harsh electron microscopy preparation with osmium tetroxide, uranyl acetate, and embedding in an epichlorohydrin derived epoxy resin (EPON) as shown in the CLEM micrographs in **Figure 3**. It turns out that the identification of the NPLs in a TEM micrographs is not as simple as thought. The NPLs are barely visible in the TEM image and could even be easily misidentified, as can be seen well in Figure 3F,G. And as already mentioned for cryo-TEM imaging, the visibility of a NPL in a TEM micrograph strongly depends on its orientation and the cellular surrounding makes identification even worse. However, one can identify the NPLs quite well by their crystallinity, as shown in **Figure 4**. Here, we used a scanning-TEM (STEM) approach which acquires a diffraction pattern at each pixel of an image, yielding a 4D dataset. With a diffraction pattern at each point it is possible to reconstruct a virtual dark field image using an arbitrary geometry of the detector area. Here, we used an annular dark field

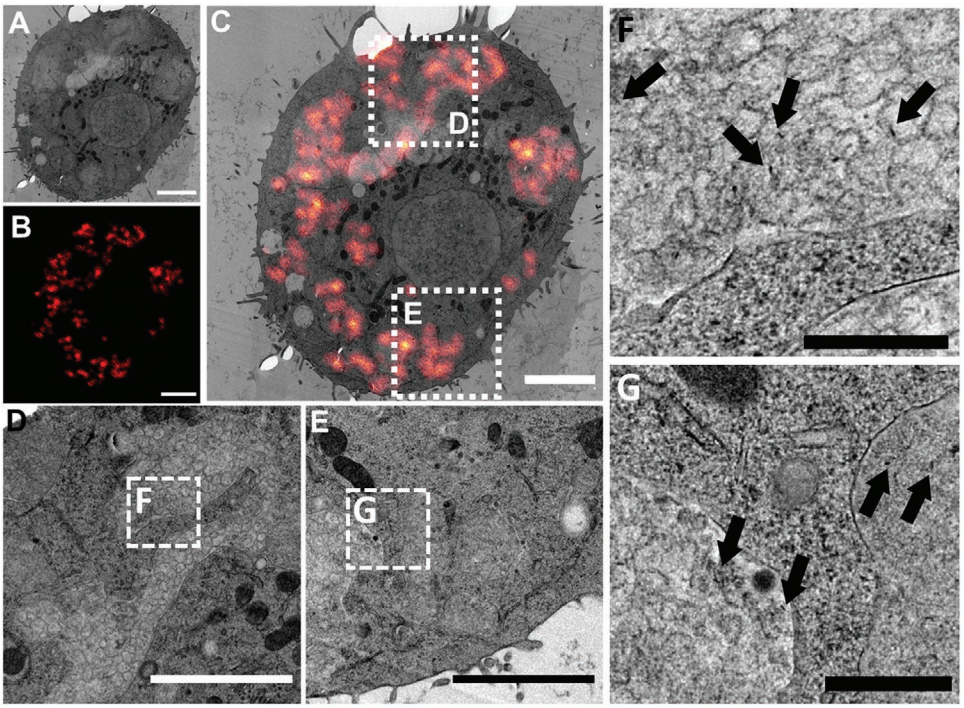

Figure 3. CLEM micrograph of BSA NCs containing NPLs (5:1) in RAW264.7 macrophages after 2 h uptake + 24 h ripening (300 µg mL^{-1}). A) Electron microscopy micrograph of one macrophage with internalized BSA NCs. B) Fluorescence microscopy micrograph of the same macrophage in (A). C) CLEM overlay of (A) and (B). D,E) Zoomed-in area of (C) showing BSA NCs in an enlarged vesicle and a late endosome. F,G) Enlargement of the indicated areas in (D) and (E). Only at these magnifications can the NPLs be seen in the TEM BF micrographs (black arrows). However, identification based on shape alone is neither very reliable nor effective, as can be seen in images (F) and (G). Scale bars: A–E: 2 µm, F,G: 500 nm.

geometry (inset in Figure 4) to reveal the position of any crystalline component. Although this method is very powerful, it is not really suitable for the identification of NPLs because it can only cover very small areas and acquisition is very time and data intensive. An alternative for the diffraction-based localization would be to use the conventional dark field method as demonstrated in Figures S10–S12, Supporting Information or using annular dark field detectors in STEM mode (Figures S13 and S14, Supporting Information). But all these methods are not very effective in terms of throughput and so it is problematic to effectively search a large area in TEM for NPLs. The same is true for analytical methods such as EELS or EDS. Here, the detection of the elements of the NPL in the presence of the cellular environment, which contains, among others, Os, U, and N, is particularly problematic. Accordingly, the most efficient way to localize the BSA NC is via the NPL fluorescence by CLEM. So, in the following we will concentrate on the morphological observations which ultimately converge into an idea of how a RAW264.7 cell processes the recorded BSA NC.

We analyzed the uptake of the nanocapsules into a macrophage in detail by TEM (Figure 3A) and fluorescence microscopy (Figure 3B). Superimposing the EM (A) with the fluorescence microscopy micrograph (B) yields the CLEM micrograph (Figure 3C). The bright fluorescence from the NPLs helps to unambiguously facilitate the localization of BSA NCs in the cell. The NCs are distributed over the whole cell except for the nucleus. We clearly localized different parts of the macrophage exhibiting accumulations of BSA NCs (D and E) showing a high fluorescence intensity. Here, the electron micrographs reveal irregular-shaped vesicles which are packed with BSA NCs (Figure 3D) as well as late endosomes, in which the structural identity of the NCs is no longer clearly recognizable (Figure 3E). These findings indicate that the NCs are processed by the cell in different manners: On the one hand there was a high accumulation of NCs in irregularly shaped, large vesicles (D) and on the other hand a degradation of the NCs (E). We captured the different processing mechanisms by varying the ripening time of the BSA NCs inside the macrophages at 2 h uptake + 0 h ripening time and 2 h uptake + 24 h ripening time. Based on our findings, we can reconstruct the processing pathway and therefore follow the track of the BSA NCs inside the cells (**Figure 5**).

Within the first 2 h of incubation, we observe the uptake of BSA NCs into RAW264.7 (Figure 5A(i) and Figure S5, Supporting Information). During this incubation phase, all events which take place during the first 120 min interval of uptake can be observed. During the incubation time we can also observe early endosomes (EE) with NCs (Figure 5B(ii) and Figure S6, Supporting Information). These findings are consistent with the cLSM images revealing that within 1 hour a co-localization of NPLs with endolysosomal compartments occurred (Figure 2E). To enable further processing of the NCs in the cells, we performed a ripening phase to complete the observation of the NCs' processing. During the 24 h ripening phase, we found BSA NCs in EE and also in densely packed late endosomes (LE) (Figure 5(ii),(iii) and Figure S7, Supporting Information). It is worth noting that these observations may change depending on the cell line. The integrity of the BSA NCs was maintained at the early stage of endocytosis, while they started to lose their integrity since the acidic environment

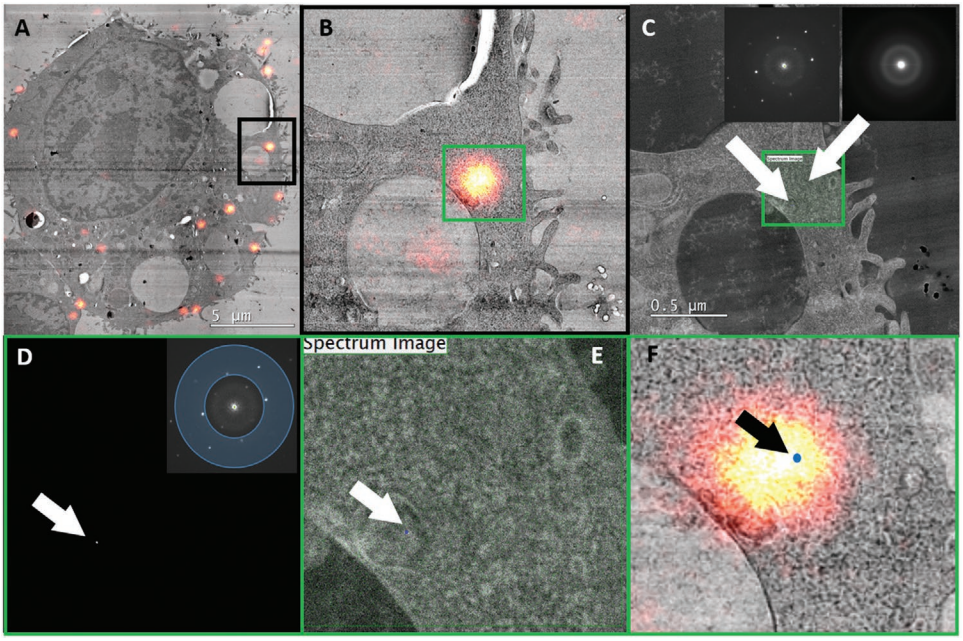

Figure 4. CLEM and diffraction imaging of NPLs. A,B) CLEM micrographs indicating the location of the NPLs from cLSM measurements (red channel). C) After cLSM measurements the area marked in green was examined using a 4D STEM approach. Each pixel of the indicated area contains a diffraction pattern. Because the NPLs are crystalline, they yield a typical diffraction pattern, as shown in the left inset of C. This diffraction was observed at the position shown by the left arrow. The whole remaining area shows only an amorphous diffraction pattern as shown for instance by the right inset. D) From the diffraction dataset it is possible to reconstruct a virtual dark field image by applying an individual mask to the diffraction data set, as shown in the inset. The dark field finally reveals the position of crystalline objects, as indicated by the white arrow. This position of the NPL can then be transferred to the E) STEM image and F) to the CLEM image. The blue dot (as indicated by the black arrow) represents the position of the NPL as identified by the diffraction imaging. The size of blue dot in (F) has been enlarged to improve the visibility. Experimental conditions: BSA NCs containing NPLs (5:1) in RAW264.7 macrophages after 10 min uptake (75 µg mL^{-1}).

in endolysosomal compartments enables the conditional degradation of the NCs (Figure 5D(iii) and Figure S4A′, Supporting Information).[25] Some LE were found to have fused with lysosomes forming endolysosomes (EL) (Figure 5E(iv) and Figure S8, in Supporting Information) where the shape integrity of the NCs was not observed anymore. The missing integrity is particularly visible in images Figure 5D′, 4E. The respective fluorescence overlays (Figure 5D,E) confirm that the endosomes contained capsules with NPLs as the endosomes appear highly fluorescent. These results indicate that the shell of the BSA NCs was impaired within 24 h by enzymatic and acidic conditions in endolysosomal compartments, which are normally revealing a dark contrast, like lysosomes, in TEM micrographs.[26] These findings are supported by previously reported observations of fully degradable protein-NCs enabling cargo release upon enzymatic cleavage leading to CD86 upregulation of bone-marrow derived dendritic cells.[27] Only at high concentrations (300 µg mL^{-1}) we found enlarged endosomes filled with NCs (Figure 5G/G′(vi) and Figure S8, Supporting Information) revealing the capsule integrity (Figure S4B′, Supporting Information). We conclude from these findings that at high capsule loadings, endosomal compartments fuse to enlarged endosomes with a big storage capacity of the NCs. The maintained capsule integrity may be explained with the pH value in the large endosomal vesicles. There, the pH is not sufficient to degrade the capsules and NCs are hindered from moving further along the pH gradient with increasing acidity. This observation indicates a kind of blockade of the degradation pathway.

In some cases, we observed NPLs in the cytosol (Figure 5F(v)). Since no freely diffusing NPLs were found neither in TEM images nor in the performed FRET experiments (Figure S1, Supporting Information), this finding is concluded to be an endosomal escape. This result is supported by the observation that the shell of the NCs degraded during endolysosomal processing and therefore releasing NPLs upon ripening.

3. Conclusion

We demonstrated that NPL containing NCs were detected and unambiguously localized in different endolysosomal compartments by CLEM. The encapsulation of the NPLs into biocompatible NCs was accomplished without disturbing the NC formation and damaging the NPLs' properties, obtaining a stable dispersion with high fluorescence intensity. We were able to adjust different NPL concentrations inside the NCs and obtained reproducible size distributions. The bright fluorescent signal in the cLSM examinations indicated that the NCs were taken up and incorporated into the macrophages used for the uptake experiments. From the CLEM data we could identify the different cell compartments containing the NCs. In this way, we could not only determine the timing of endolysosomal co-localization, but also trace the NCs in each compartment. We show that the NCs are processed at three different locations upon the endolysosomal pathway: The NC shell was impaired

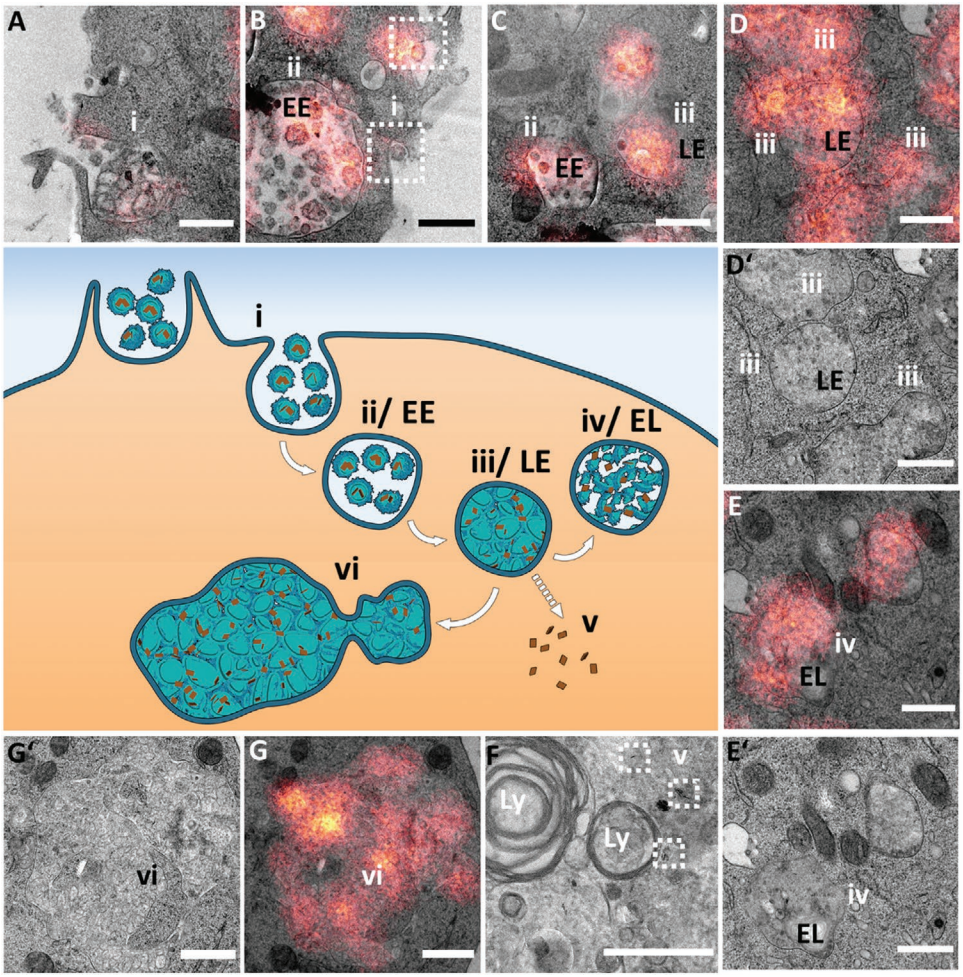

Figure 5. Compilation of the intracellular fate of BSA NCs (1:5 loading ratio) by TEM micrographs. A) Uptake event (i) of BSA NCs in a cell captured after 2 h incubation B) Uptake event (i) and early endosome (ii/EE) of BSA NCs captured after 2 h incubation. C) Early endocytosis of BSA NCs (ii) and a late endosome (iii/LE) with BSA NCs after 2 h incubation + 24 h ripening. D) Late endosomes (LE) with BSA NCs visible after 2 h incubation + 24 h ripening. E) Degradation of BSA NCs in an endolysosome (iv/EL) after 2 h incubation + 24 h ripening F) Escaped NPLs (v) captured after 24 h ripening. Ly: lysosome G) Enlarged endosome with BSA NCs at high concentration (300 µg/mL) after 2 h incubation + 24 h ripening D′, E′ and G′ correspond to the same respective EM images without fluorescence correlation. Scale bars: 500 nm.

in late endosomes, indicating degradation, the NCs were stored in large endosomes at high capsule concentrations revealing an intact shell, and we observed an endolysosomal escape which is crucial for the successful delivery of a potential drug encapsulated inside the BSA NCs. The findings are very important for future research on cell uptake mechanisms and may reveal the metabolic pathway of an encapsulated drug.

Supporting Information

Supporting Information is available from the Wiley Online Library or from the author.

Acknowledgements

M.L.F. and S.H. contributed equally to this work. The authors would like to thank Christoph Sieber for his assistance with the HPF and the preparation of the ultramicrotome sections, Renate van Brandwijk-Peterhans for her support in all the cell culture matters, Dr. Johanna Simon for performing the FACS measurements, Christine Rosenauer for DLS measurements, and Elke Muth for zeta potential measurements. H.H. thanks the support by the Max Planck Graduate Center with the Johannes Gutenberg-Universität Mainz (MPGC). The authors thank the financial support funded by the Deutsche Forschungsgemeinschaft (DFG, German Research Foundation)—Project-ID 213555243—SFB1066.

Open access funding enabled and organized by Projekt DEAL.

Conflict of Interest

The authors declare no conflict of interest.

Data Availability Statement

The data that support the findings of this study are available from the corresponding author upon reasonable request.

Keywords

correlative microscopy, drug delivery, intracellular pathways, protein nanocarriers, transmission electron microscopy

Received: October 7, 2021
Revised: January 18, 2022
Published online: February 27, 2022

[1] M. Ferrari, *Nat. Rev. Cancer* **2005**, *5*, 161.
[2] C. L. Ventola, *P T* **2017**, *42*, 742.
[3] E. Beltrán-Gracia, A. López-Camacho, I. Higuera-Ciapara, J. B. Velázquez-Fernández, A. A. Vallejo-Cardona, *Nanomedicine Review: Clinical Developments in Liposomal Applications*, Springer, Vienna **2019**.
[4] A. C. Anselmo, S. Mitragotri, *Bioeng. Transl. Med.* **2019**, *4*, e10143.
[5] K. Landfester, A. Musyanovych, V. Mailänder, *J. Polym. Sci. Part A: Polym. Chem.* **2010**, *48*, 493.
[6] K. Landfester, V. Mailänder, *Expert Opin. Drug Deliv.* **2013**, *10*, 593.
[7] K. Piradashvili, M. Fichter, K. Mohr, S. Gehring, F. R. Wurm, K. Landfester, *Biomacromolecules* **2015**, *16*, 815.
[8] M.-L. Frey, J. Simon, M. Brückner, V. Mailänder, S. Morsbach, K. Landfester, *Polym. Chem.* **2020**, *11*, 3821.
[9] P. Foroozandeh, A. A. Aziz, *Nanoscale Res. Lett.* **2018**, *13*, 339.
[10] J. Reinholz, K. Landfester, V. Mailänder, *Drug Delivery* **2018**, *25*, 1694.
[11] F. J. Hsieh, Y. Chen, Y. Huang, H. Lee, C. Lin, H. Chang, *Anal. Chem.* **2018**, *90*, 1566.
[12] N. Prabhakar, M. Peurla, S. Koho, T. Deguchi, T. Nareoja, H. Chang, J. Rosenholm, P. Hanninen, *Small* **2018**, *14*.
[13] S. Han, M. Raabe, L. Hodgson, J. Mantell, P. Verkade, T. Lasser, K. Landfester, T. Weil, I. Lieberwirth, *Nano Lett.* **2019**, *19*, 2178.
[14] B. Dubertret, P. Skourides, D. J. Norris, V. Noireaux, A. H. Brivanlou, A. Libchaber, *Science* **2002**, *298*, 1759.
[15] M. Seleci, D. Ag Seleci, T. Scheper, F. Stahl, *Int. J. Mol. Sci.* **2017**, *18*, 1415.
[16] C. Mi, Y. Wang, J. Zhang, H. Huang, L. Xu, S. Wang, X. Fang, J. Fang, C. Mao, S. Xu, *J. Biotechnol.* **2011**, *153*, 125.
[17] K. V. P. Kumar, O. S. N. Ghosh, G. Balakrishnan, P. Thiru gnanasambantham, S. K. Raghavan, A. K. Viswanath, *RSC Adv.* **2015**, *5*, 16815.
[18] M. J. D. Clift, C. Brandenberger, B. Rothen-Rutishauser, D. M. Brown, V. Stone, *Toxicology* **2011**, *286*, 58.
[19] H. Halim, J. Simon, I. Lieberwirth, V. Mailänder, K. Koynov, A. Riedinger, *J. Mater. Chem. B* **2020**, *8*, 146.
[20] H. Schlaad, H. Kukula, J. Rudloff, I. Below, *Macromolecules* **2001**, *34*, 4302.
[21] H. Xu, L. Shen, L. Xu, Y. Yang, *Biomed. Microdevices* **2015**, *17*, 8.
[22] H. Halim, D. Trieb, N. Huber, M. Martínez-Negro, L.-A. Meyer, T. Basché, S. Morsbach, K. A. I. Zhang, A. Riedinger, *J. Phys. Chem. C* **2020**, *124*, 25028.
[23] O. Erdem, K. Gungor, B. Guzelturk, I. Tanriover, M. Sak, M. Olutas, D. Dede, Y. Kelestemur, H. V. Demir, *Nano Lett.* **2019**, *19*, 4297.
[24] S. Jiang, M. Xiao, W. Sun, D. Crespy, V. Mailaender, X. Peng, J. Fan, K. Landfester, *Angew. Chem., Int. Ed.* **2020**, *59*, 20008.
[25] N. A. Bright, L. J. Davis, J. P. Luzio, *Curr. Biol.* **2016**, *26*, 2233.
[26] D. Aston, R. A. Capel, K. L. Ford, H. C. Christian, G. R. Mirams, E. A. Rog-Zielinska, P. Kohl, A. Galione, R. A. B. Burton, D. A. Terrar, *Sci. Rep.* **2017**, *7*, 40620.
[27] K. Piradashvili, J. Simon, D. Paßlick, J. R. Höhner, V. Mailänder, F. R. Wurm, K. Landfester, *Nanoscale Horiz.* **2017**, *2*, 297.